

gfnx: Fast and Scalable Library for Generative Flow Networks in JAX

D. Tiapkin¹, A. Agarkov², N. Morozov², I. Maksimov²,
 A. Tsyganov², T. Gritsaev^{3,2}, and S. Samsonov²

¹École Polytechnique, Palaiseau, France

²HSE University, Moscow, Russia

³Constructor University, Bremen, Germany

Abstract

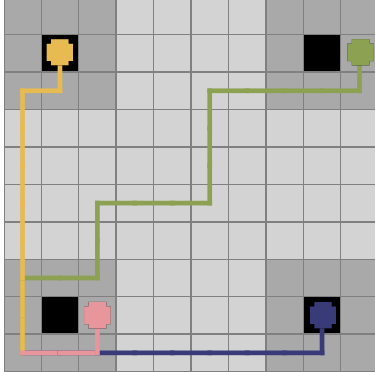
In this paper, we present `gfnx`, a fast and scalable package for training and evaluating Generative Flow Networks (GFlowNets) written in JAX. `gfnx` provides an extensive set of environments and metrics for benchmarking, accompanied with single-file implementations of core objectives for training GFlowNets. We include synthetic hypergrids, multiple sequence generation environments with various editing regimes and particular reward designs for molecular generation, phylogenetic tree construction, Bayesian structure learning, and sampling from the Ising model energy. Across different tasks, `gfnx` achieves significant wall-clock speedups compared to Pytorch-based benchmarks (such as `torchgfn` library [39]) and author implementations. For example, `gfnx` achieves up to 55 times speedup on CPU-based sequence generation environments, and up to 80 times speedup with the GPU-based Bayesian network structure learning setup. Our package provides a diverse set of benchmarks and aims to standardize empirical evaluation and accelerate research and applications of GFlowNets. The library is available on GitHub (<https://github.com/d-tiapkin/gfnx>) and on pypi (<https://pypi.org/project/gfnx/>). Documentation is available on <https://gfnx.readthedocs.io>.

1 Introduction

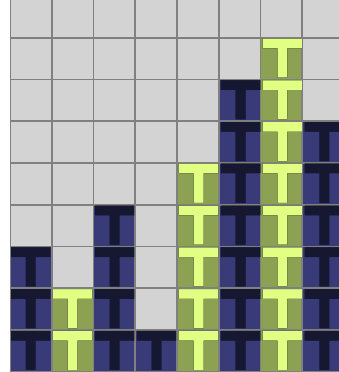
Many problems in machine learning and scientific discovery require drawing samples from complex, discrete distributions, often known only up to a normalizing constant. The well-known solution to this problem is to use MCMC methods [51, 60]. These methods typically require many sampling steps to converge, making them prohibitively costly as the problem scale increases. The *amortized sampling* approach provides an alternative: instead of running an MCMC sampler, one trains a generative model to perform *approximate* sampling from the target distribution. A recent class of models addressing this problem is given by the *Generative Flow Networks* (GFlowNets, GFNs, [2]). GFlowNets have shown promising results across a broad range of domains, such as phylogenetic tree generation [72], crystal structure discovery [47, 52], biological sequence design [29, 69], and molecular generation [38, 63].

Mathematical foundations of GFlowNets were established in [2, 3]. Recent works establish connections between GFlowNets and (hierarchical) variational inference algorithms [45], and formalize their connections with reinforcement learning (RL) [65, 48, 15], particularly with a class of RL

*daniil.tiapkin@polytechnique.edu, aagarkov@hse.ru, nvmorozov@hse.ru, yvmaksimov@hse.ru, atsyganov@hse.ru, tgritsaev@constructor.university, svsamsonov@hse.ru



(a) 2D Hypergrid environment.



(b) Bit Sequence environment.

Figure 1: Visualization of GFlowNet environments. The first figure illustrates four sample trajectories, each represented by distinct colored paths from initial to terminal states. The second figure illustrates the sequential construction of a bit string; each row corresponds to a different environment state: the first row represents the empty string (initial state), the last row the complete string (final state), and intermediate rows display the token-by-token generation process.

problems with entropy regularization. Given these important contributions, the majority of recent papers have focused on applications of GFlowNets to particular problems, raising a need for a scalable and standardized benchmark package to evaluate new methods.

Several libraries provide GFlowNet training and environment frameworks, including `torchgfn` [39], `recursionpharma/gfownet` [59], and `alexhernandezgarcia/gfownet` [23]. These toolkits implement essential functionalities and offer helpful abstractions, but they share a common limitation: environment logic typically executes on the host (CPU) and thus does not fully leverage specialized hardware acceleration. As a result, data must be repeatedly transferred between CPU and accelerator hardware (GPU or TPU), creating a performance bottleneck during training.

Recent trends in RL research highlight that runtime efficiency is critical for developing new algorithms. Fast environments allow rapid iteration, large-scale hyperparameter sweeps, and more reliable statistical comparisons across random seeds [41, 28, 11, 32, 16]. A key technique enabling such acceleration is just-in-time (JIT) compilation of the entire training loop, achievable through JAX [6]. This approach has led to substantial speedups across RL systems [41, 61, 5, 64, 12, 55], supported by a vast ecosystem of JAX-native environments and tools [17, 40, 37, 4, 46, 53, 66, 13].

Our contribution. In this work, we introduce a JAX-based library for GFlowNets. Our goal is to bring JAX-compiled environments and training utilities to the GFlowNet community, enabling accelerated research and offering efficient experimental pipelines. The library also follows the "single-file" design philosophy of CleanRL [25], providing a clear and reliable baseline implementation.

2 Library Details

The core of the `gfnx` library consists of JIT-able environments, reward modules, and success metrics implemented entirely in JAX [6]. Each component is documented on <https://gfnx.readthedocs.io> with the corresponding source papers, usage examples, and explanatory notes.

For every environment, we provide a concise, single-file JAX baseline that mirrors the simplicity and hackability of CleanRL [25]. These examples rely on `Equinox` [33] for neural networks and

are JIT-compiled end-to-end together with the environment, following the practices popularized by `purejaxrl` [41].

Library architecture. The main part of the library is organized into the following modules:

- `base.py` — Defines the shared primitives (`BaseEnvState`, `BaseEnvParams`, `BaseVecEnvironment`, `BaseRewardModule`) and their typing aliases that appear throughout the codebase.
- `environment/` — Implements vectorized, JITable environments derived from `BaseVecEnvironment`, pairing an `EnvState` to hold mutable state with `EnvParams` that configure dynamics and bind reward modules.
- `reward/` — Implements reward modules and likelihood/prior components for each environment. By decoupling rewards from dynamics we support swapping reward families or learning them during GFlowNet training without recompiling environment logic.
- `metrics/` — Provides success metrics for monitoring sampling quality. Multiple metrics highlight how GFlowNet evaluation differs from standard RL, where raw return is the main score.
- `utils/` — Gathers helper routines ranging from environment-specific utilities to reusable tools such as `gfnx.utils.forward_rollout`, which produces trajectories for any fixed environment.

In addition, the repository offers the following companion code outside the core package, intended as stable, hackable examples rather than prescriptive frameworks:

- `baselines/` — Single-file, end-to-end JAX training scripts that demonstrate fast compiled loops and provide reproducible implementations of established algorithms.
- `proxy/` — Utilities for training dataset-driven proxy reward models; these scripts tie into the AMP environment section for deeper discussion.

Together these components emphasize modularity, full JAX compatibility, and a hackable workflow that lowers the barrier to experimenting with new GFlowNet ideas.

We highlight a few implementation details:

- Following the JAX paradigm, environments are *stateless*; all mutable data lives in the `EnvState` object returned by `env.reset` and modified explicitly by each `env.step`.
- Environments are vectorized to simplify reward evaluation. We only evaluate rewards when at least one element of the batch is terminal by wrapping the computation in `jax.lax.cond`, which avoids the redundant work that a naive `jax.vmap` over terminal checks would incur.
- Instead of returning raw rewards, environments emit `log_reward`: terminal transitions yield their log-reward, while non-terminal steps return zero. Log-scale rewards align with how most GFlowNet algorithms consume the signal.

Example. A short example from the documentation illustrates how to instantiate the Hypergrid environment, roll it forward, and use the stop action:

Listing 1: Minimal Hypergrid usage in gfnx.

```

import jax
import jax.numpy as jnp
import gfnx

# 1. Pick a reward module;
reward = gfnx.EasyHypergridRewardModule()

# 2. Create the environment. Need to pass a corresponding reward module
env = gfnx.HypergridEnvironment(reward_module=reward, dim=3, side=5)
params = env.init(jax.random.PRNGKey(0))

# 3. Reset to get the initial observation/state batch.
obs, state = env.reset(num_envs=1, env_params=params)

# 4. Take a forward step (increment coordinate 0).
action = jnp.array([0], dtype=jnp.int32)
obs, state, log_reward, done, _ = env.step(state, action, params)

print("Terminal?", bool(state.is_terminal[0])) # returns False
print("Reward (log scale):", float(log_reward[0])) # return 0

# 5. Stop when you are ready to terminate the trajectory. Stop action is the last action.
stop = jnp.array([env.action_space.n - 1], dtype=jnp.int32)
obs, state, log_reward, done, _ = env.step(state, stop, params)

print("Terminal?", bool(state.is_terminal[0])) # returns True
print("Reward (log scale):", float(log_reward[0])) # returns a corresponding log-reward

```

Comparison with torchgfn. `torchgfn` ships with tightly integrated training and environment stacks, whereas `gfnx` deliberately decouples these pieces so researchers can mix and match environment logic, reward modules, and training code. This separation trades the ready-made training loops of `torchgfn` for greater flexibility when running fully on-device execution or embedding the environments inside custom trainers.

Listing 2: Example of backward transitions in gfnx.

```

# 1. Reset the environment
obs, state = env.reset(num_envs=1, env_params=params)

# 2. Take a forward step (increment coordinate 0).
action = jnp.array([0], dtype=jnp.int32)
next_obs, next_state, log_reward, done, _ = env.step(state, action, params)

# 3. Compute a corresponding backward action
bwd_action = env.get_backward_action(state, action, next_state, params)

# 4. Make a backward step
_, prev_next_state, _, _, _ = env.backward_step(next_state, bwd_action, params)

# 5. Verify that we indeed inverted the action
import chex; chex.assert_trees_all_equal(state, prev_next_state) # Do not raise error

```

The libraries also diverge in how they treat backward actions: `torchgfn` defines a backward move

as an inverse to every forward transition (e.g., "remove a particular symbol on a particular position" in sequence generation), while `gfnx` abstracts backward actions to the structural choices alone (e.g., "remove any character on a particular position"). This abstraction mirrors our broader design goal of keeping the environment design as flexible as possible. We intentionally design backward transitions to mirror their forward counterparts as closely as possible, which makes it easy to reason about state reversibility and implement symmetric training objectives. In particular, this symmetry allows us to implement a backward rollout by only replacing the initial states by terminal ones and `env.step` by `env.backward_step`.

3 Environments and Runtime

`gfnx` implements a wide range of environments from GFlowNet literature:

1. **Hypergrids** [2]. This environment is a d -dimensional discrete hypercube of side length H . There are actions that increment a single coordinate by 1 while remaining in the grid and a stop action. The reward concentrates in high-reward regions near the corners of the hypercube, with substantially lower rewards elsewhere.
2. **Bit sequences** [65]. In this environment our goal is to sample bit strings of a fixed length n in non-autoregressive manner (See Appendix B.2 for a discussion on different generation schemes for sequences). The string is split into k -bit blocks, and an empty token is initially put into each position. The generation process replaces an empty token with a k -bit word at each step until no empty tokens remain in the sequence. The vocabulary is, therefore, predefined as well as the mode set which we use for evaluation setup. The reward is defined through Hamming distance to the closest mode.
3. **TFBind8** [62]. TFBind8 environment evaluates DNA sequence design, where the goal is to generate sequences of nucleotides. The reward is wet-lab measured DNA binding activity to a human transcription factor, SIX6 [1]. Formally, this is an autoregressive sequence generation environment of fixed length 8 with a vocabulary of size 4 (corresponding to nucleotides).
4. **QM9** [62]. QM9 is a small molecule generation environment. We adopt the prepend/append sequence formulation, which models the generation process using 11 building blocks with 2 stems, producing molecules of 5 blocks. Rewards are given by a proxy model trained to predict the HOMO-LUMO gap, an important molecular property [71].
5. **AMP** [29]. In the AMP task, our objective is to generate peptides with antimicrobial properties. We model this as an autoregressive environment with variable-length sequences (up to 60 tokens) over a 20–amino acid vocabulary. The environment provides rewards from a proxy model trained on the DBAASP database [57].
6. **Phylogenetic trees** [72]. The environment starts from a forest of n singleton species and proceeds by repeatedly merging two subtrees into a new common ancestor. The trajectory has a fixed length of $n - 1$ steps, after which a rooted binary tree is formed. States correspond to intermediate forests and actions to pairwise merges. The terminal reward induces a Gibbs distribution that favors trees requiring fewer mutations. Only the tree topology is modeled, with branch lengths excluded.
7. **Bayesian structure learning** [14]. The environment constructs a Directed Acyclic Graph by sequentially adding edges while enforcing acyclicity. Any state may be terminal, with the

reward equal to the log-posterior under linear-Gaussian or BGe scores. Datasets are generated from an Erdős–Rényi ground-truth graph using a linear-Gaussian model.

8. **Ising model** [70]. The environment represents partial spin assignments of a lattice, with states given by ternary vectors $s \in \{-1, +1, \emptyset\}^{N \times N}$ and initial state containing only unassigned sites (i.e. \emptyset). At each step, an action chooses an unassigned site and sets its spin to -1 or $+1$, producing a full configuration after N^2 steps. The reward corresponds to the Gibbs distribution of an Ising model with energy function $\mathcal{E}_J(\mathbf{x}) = -\mathbf{x}^\top J \mathbf{x}$, where $J \in \mathbb{R}^{N^2 \times N^2}$, and $\mathbf{x} \in \mathbb{R}^{N^2}$.

Runtime comparisons of our library with standard baselines are listed in Table 1. Some environments are sufficiently small to allow benchmarking on a CPU, while others are benchmarked on a GPU. The `gfnx` implementation achieves up to an 80-fold speedup on the Bayesian structure learning environment (GPU) and up to a 55-fold speedup on the QM9 environment (CPU).

Environment	Baseline Impl.	Device	Objective	Baseline	<code>gfnx</code>
Hypergrid ($20 \times 20 \times 20 \times 20$)	[39]	CPU	DB	178.3 ± 2.0 it/s	1560.0 ± 3.6 it/s
			TB	219.9 ± 1.1 it/s	1463.3 ± 1.4 it/s
			SubTB	121.0 ± 0.7 it/s	596.0 ± 0.3 it/s
Bitseq ($n = 120, k = 8$)	[65]	GPU	DB	52.4 ± 0.8 it/s	1666.4 ± 8.0 it/s
			TB	54.0 ± 0.2 it/s	2433.6 ± 67.1 it/s
TFBind8	[62]	CPU	TB	230.4 ± 2.7 it/s	6929.3 ± 26.0 it/s
QM9	[62]	CPU	TB	162.3 ± 1.5 it/s	9061.6 ± 28.7 it/s
AMP	[29]	GPU	TB	21.2 ± 1.7 it/s	413.1 ± 3.4 it/s
Phylogenetic Trees (DS-1) Phylogenetic Trees (DS-2) Phylogenetic Trees (DS-3) Phylogenetic Trees (DS-4) Phylogenetic Trees (DS-5) Phylogenetic Trees (DS-6) Phylogenetic Trees (DS-7) Phylogenetic Trees (DS-8)	[15]	GPU	FLDB	13.3 ± 0.7 it/s	263.6 ± 2.1 it/s
				9.9 ± 0.1 it/s	208.4 ± 4.0 it/s
				8.6 ± 0.1 it/s	149.7 ± 2.4 it/s
				10.0 ± 0.1 it/s	122.0 ± 1.0 it/s
				11.7 ± 0.7 it/s	76.1 ± 0.9 it/s
				6.3 ± 0.3 it/s	66.3 ± 1.4 it/s
				2.9 ± 0.1 it/s	36.7 ± 0.4 it/s
				4.1 ± 0.2 it/s	39.1 ± 0.6 it/s
Structure Learning	[39]	GPU	MDB	0.73 ± 0.03 it/s	58.0 ± 1.0 it/s
Ising model ($N = 9$)	–	GPU	TB	–	27.8 ± 0.2 it/s
Ising model ($N = 10$)	–	GPU	TB	–	26.4 ± 0.6 it/s

Table 1: Iterations per second comparison between baseline and `gfnx` implementations on GFlowNet environments. Higher values indicate better performance. We add the 3 sigma standard error interval for time performance. For Ising model we implemented the EBM setting from [70], which had no available open-source implementations.

Full comparisons with implementations from previous literature across various metrics, along with detailed experimental setups, are presented in Section B.

4 Conclusion & Future Work

Overall, `gfnx` provides a suite of JAX-native environments, reward modules, and metrics that speeds up amortized-sampling research while preserving the transparency needed for reproducible benchmarks. The single-file, end-to-end compiled baselines run up to $80\times$ faster than comparable non-JAX implementations without degrading sampling quality, lowering the barrier to rapid experimentation. Despite this progress, several gaps remain and motivate further developments:

- *Continuous action spaces*: in the current form, `gfnx` supports only discrete action spaces, yet many problems, such as a more complete version of phylogenetic tree generation environment [72] also have continuous components;
- *Non-acyclic environments*: many natural problems, such as permutation generation, might be more clearly written without an acyclicity constraint [7, 49];
- *Multi-objective support*: the need to generate diverse Pareto optimal solutions in multi-objective scenarios also arises in many problems [30, 8];
- *Additional baselines*: GFlowNets can be successfully trained with various entropy-regularized RL algorithms [65, 15, 48, 50, 21]. It will also be valuable to implement backward policy optimization algorithms [31, 20] and exploration techniques [35, 42, 34] that were shown to have various benefits for GFlowNet training;
- *Trainer vectorization*: batching over seeds and hyperparameters, in the style of `purejaxrl` [41], would improve reproducibility and hyperparameter sweeps on small environments.

References

- [1] Luis A Barrera, Anastasia Vedenko, Jesse V Kurland, Julia M Rogers, Stephen S Gisselbrecht, Elizabeth J Rossin, Jaie Woodard, Luca Mariani, Kian Hong Kock, Sachi Inukai, et al. Survey of variation in human transcription factors reveals prevalent dna binding changes. *Science*, 351(6280):1450–1454, 2016.
- [2] Emmanuel Bengio, Moksh Jain, Maksym Korablyov, Doina Precup, and Yoshua Bengio. Flow network based generative models for non-iterative diverse candidate generation. *Advances in Neural Information Processing Systems*, 34:27381–27394, 2021.
- [3] Yoshua Bengio, Salem Lahlou, Tristan Deleu, Edward J. Hu, Mo Tiwari, and Emmanuel Bengio. Gflownet foundations. *Journal of Machine Learning Research*, 24(210):1–55, 2023.
- [4] Clément Bonnet, Daniel Luo, Donal Byrne, Shikha Surana, Sasha Abramowitz, Paul Duckworth, Vincent Coyette, Laurence I. Midgley, Elshadai Tegegn, Tristan Kalloniatis, Omayma Mahjoub, Matthew Macfarlane, Andries P. Smit, Nathan Grinsztajn, Raphael Boige, Cemlyn N. Waters, Mohamed A. Mimouni, Ulrich A. Mbou Sob, Ruan de Kock, Siddarth Singh, Daniel Furelos-Blanco, Victor Le, Arnu Pretorius, and Alexandre Laterre. Jumanji: a diverse suite of scalable reinforcement learning environments in jax, 2024.
- [5] Michał Bortkiewicz, Władysław Pałucki, Vivek Myers, Tadeusz Dziarmaga, Tomasz Arczewski, Łukasz Kuciński, and Benjamin Eysenbach. Accelerating goal-conditioned reinforcement learning algorithms and research. In *The Thirteenth International Conference on Learning Representations*, 2025.

[6] James Bradbury, Roy Frostig, Peter Hawkins, Matthew James Johnson, Chris Leary, Dougal Maclaurin, George Necula, Adam Paszke, Jake VanderPlas, Skye Wanderman-Milne, and Qiao Zhang. JAX: composable transformations of Python+NumPy programs, 2018.

[7] Leo Brunswic, Yinchuan Li, Yushun Xu, Yijun Feng, Shangling Jui, and Lizhuang Ma. A theory of non-acyclic generative flow networks. In *Proceedings of the AAAI Conference on Artificial Intelligence*, volume 38, pages 11124–11131, 2024.

[8] Yihang Chen and Lukas Mauch. Order-preserving gflownets. In *The Twelfth International Conference on Learning Representations*, 2023.

[9] David Chickering, Dan Geiger, and David Heckerman. Learning Bayesian Networks: Search Methods and Experimental Results. In *Proceedings of Fifth Conference on Artificial Intelligence and Statistics*, 1995.

[10] David Maxwell Chickering. Optimal Structure Identification With Greedy Search. *Journal of Machine Learning Research*, 2002.

[11] Cédric Colas, Olivier Sigaud, and Pierre-Yves Oudeyer. How many random seeds? statistical power analysis in deep reinforcement learning experiments, 2018.

[12] Samuel Coward, Michael Beukman, and Jakob Foerster. Jaxued: A simple and useable ued library in jax. *arXiv preprint*, 2024.

[13] DeepMind, Igor Babuschkin, Kate Baumli, Alison Bell, Surya Bhupatiraju, Jake Bruce, Peter Buchlovsky, David Budden, Trevor Cai, Aidan Clark, Ivo Danihelka, Antoine Dedieu, Claudio Fantacci, Jonathan Godwin, Chris Jones, Ross Hemsley, Tom Hennigan, Matteo Hessel, Shaobo Hou, Steven Kapturowski, Thomas Keck, Iurii Kemaev, Michael King, Markus Kunesch, Lena Martens, Hamza Merzic, Vladimir Mikulik, Tamara Norman, George Papamakarios, John Quan, Roman Ring, Francisco Ruiz, Alvaro Sanchez, Laurent Sartran, Rosalia Schneider, Eren Sezener, Stephen Spencer, Srivatsan Srinivasan, Miloš Stanojević, Wojciech Stokowiec, Luyu Wang, Guangyao Zhou, and Fabio Viola. The DeepMind JAX Ecosystem, 2020.

[14] Tristan Deleu, António Góis, Chris Emezue, Mansi Rankawat, Simon Lacoste-Julien, Stefan Bauer, and Yoshua Bengio. Bayesian structure learning with generative flow networks. In *Uncertainty in Artificial Intelligence*, pages 518–528. PMLR, 2022.

[15] Tristan Deleu, Padideh Nouri, Nikolay Malkin, Doina Precup, and Yoshua Bengio. Discrete probabilistic inference as control in multi-path environments. In *The 40th Conference on Uncertainty in Artificial Intelligence*, 2024.

[16] Theresa Eimer, Marius Lindauer, and Roberta Raileanu. Hyperparameters in reinforcement learning and how to tune them. In *International conference on machine learning*, pages 9104–9149. PMLR, 2023.

[17] C. Daniel Freeman, Erik Frey, Anton Raichuk, Sertan Girgin, Igor Mordatch, and Olivier Bachem. Brax - a differentiable physics engine for large scale rigid body simulation, 2021.

[18] Nir Friedman and Daphne Koller. Being Bayesian About Network Structure. A Bayesian Approach to Structure Discovery in Bayesian Networks. *Machine Learning*, 2003.

[19] Dan Geiger and David Heckerman. Learning gaussian networks. In *Uncertainty in Artificial Intelligence*, pages 235–243. Elsevier, 1994.

[20] Timofei Gritsaev, Nikita Morozov, Sergey Samsonov, and Daniil Tiapkin. Optimizing backward policies in GFlownets via trajectory likelihood maximization. In *The Thirteenth International Conference on Learning Representations*, 2025.

[21] Haoran He, Emmanuel Bengio, Qingpeng Cai, and Ling Pan. Random policy evaluation uncovers policies of generative flow networks. In Aarti Singh, Maryam Fazel, Daniel Hsu, Simon Lacoste-Julien, Felix Berkenkamp, Tegan Maharaj, Kiri Wagstaff, and Jerry Zhu, editors, *Proceedings of the 42nd International Conference on Machine Learning*, volume 267 of *Proceedings of Machine Learning Research*, pages 22351–22367. PMLR, 13–19 Jul 2025.

[22] David Heckerman, Dan Geiger, and David M Chickering. Learning bayesian networks: The combination of knowledge and statistical data. *Machine learning*, 1995.

[23] Alex Hernandez-Garcia, Nikita Saxena, Alexandra Volokhova, Michał Koziarski, Divya Sharma, Joseph D Viviano, Pierre Luc Carrier, and Victor Schmidt. gflownet, 2024.

[24] Geoffrey E Hinton. Training products of experts by minimizing contrastive divergence. *Neural computation*, 14(8):1771–1800, 2002.

[25] Shengyi Huang, Rousslan Fernand Julien Dossa, Chang Ye, Jeff Braga, Dipam Chakraborty, Kinal Mehta, and João G.M. Araújo. Cleanrl: High-quality single-file implementations of deep reinforcement learning algorithms. *Journal of Machine Learning Research*, 23(274):1–18, 2022.

[26] Koji Hukushima and Koji Nemoto. Exchange monte carlo method and application to spin glass simulations. *Journal of the Physical Society of Japan*, 65(6):1604–1608, 1996.

[27] Ernst Ising. Beitrag zur theorie des ferromagnetismus. *Zeitschrift für Physik*, 31(1):253–258, 1925.

[28] Matthew Thomas Jackson, Chris Lu, Louis Kirsch, Robert Tjarko Lange, Shimon Whiteson, and Jakob Nicolaus Foerster. Discovering temporally-aware reinforcement learning algorithms. In *The Twelfth International Conference on Learning Representations*, 2024.

[29] Moksh Jain, Emmanuel Bengio, Alex Hernandez-Garcia, Jarrid Rector-Brooks, Bonaventure FP Dossou, Chanakya Ajit Ekbote, Jie Fu, Tianyu Zhang, Michael Kilgour, Dinghuai Zhang, et al. Biological sequence design with gflownets. In *International Conference on Machine Learning*, pages 9786–9801. PMLR, 2022.

[30] Moksh Jain, Sharath Chandra Raparthy, Alex Hernández-García, Jarrid Rector-Brooks, Yoshua Bengio, Santiago Miret, and Emmanuel Bengio. Multi-objective gflownets. In *International Conference on Machine Learning*, pages 14631–14653. PMLR, 2023.

[31] Hyosoon Jang, Yunhui Jang, Minsu Kim, Jinkyoo Park, and Sungsoo Ahn. Pessimistic backward policy for gflownets. In *Advances in Neural Information Processing Systems*, volume 37, pages 107087–107111. Curran Associates, Inc., 2024.

[32] Scott M. Jordan, Adam White, Bruno Castro Da Silva, Martha White, and Philip S. Thomas. Position: Benchmarking is limited in reinforcement learning research. In Ruslan Salakhutdinov, Zico Kolter, Katherine Heller, Adrian Weller, Nuria Oliver, Jonathan Scarlett, and Felix

Berkenkamp, editors, *Proceedings of the 41st International Conference on Machine Learning*, volume 235 of *Proceedings of Machine Learning Research*, pages 22551–22569. PMLR, 21–27 Jul 2024.

[33] Patrick Kidger and Cristian Garcia. Equinox: neural networks in JAX via callable PyTrees and filtered transformations. *Differentiable Programming workshop at Neural Information Processing Systems 2021*, 2021.

[34] Minsu Kim, Sanghyeok Choi, Taeyoung Yun, Emmanuel Bengio, Leo Feng, Jarrid Rector-Brooks, Sungsoo Ahn, Jinkyoo Park, Nikolay Malkin, and Yoshua Bengio. Adaptive teachers for amortized samplers. In *The Thirteenth International Conference on Learning Representations*, 2025.

[35] Minsu Kim, Taeyoung Yun, Emmanuel Bengio, Dinghuai Zhang, Yoshua Bengio, Sungsoo Ahn, and Jinkyoo Park. Local search gflownets. In *The Twelfth International Conference on Learning Representations*, 2023.

[36] Daphne Koller and Nir Friedman. *Probabilistic Graphical Models: Principles and Techniques*. MIT press, 2009.

[37] Sotetsu Koyamada, Shinri Okano, Soichiro Nishimori, Yu Murata, Keigo Habara, Haruka Kita, and Shin Ishii. Pgx: Hardware-accelerated parallel game simulators for reinforcement learning. In *Advances in Neural Information Processing Systems*, volume 36, pages 45716–45743, 2023.

[38] MichałKoziarski, Andrei Rekesh, Dmytro Shevchuk, Almer van der Sloot, Piotr Gaiński, Yoshua Bengio, Cheng-Hao Liu, Mike Tyers, and Robert A. Batey. Rgfn: Synthesizable molecular generation using gflownets. In A. Globerson, L. Mackey, D. Belgrave, A. Fan, U. Paquet, J. Tomczak, and C. Zhang, editors, *Advances in Neural Information Processing Systems*, volume 37, pages 46908–46955. Curran Associates, Inc., 2024.

[39] Salem Lahlou, Joseph D Viviano, and Victor Schmidt. torchgfn: A pytorch gflownet library. *arXiv preprint arXiv:2305.14594*, 2023.

[40] Robert Tjarko Lange. gymax: A JAX-based reinforcement learning environment library, 2022.

[41] Chris Lu, Jakub Kuba, Alistair Letcher, Luke Metz, Christian Schroeder de Witt, and Jakob Foerster. Discovered policy optimisation. *Advances in Neural Information Processing Systems*, 35:16455–16468, 2022.

[42] Kanika Madan, Alex Lamb, Emmanuel Bengio, Glen Berseth, and Yoshua Bengio. Towards improving exploration through sibling augmented gflownets. In *The Thirteenth International Conference on Learning Representations*, 2025.

[43] Kanika Madan, Jarrid Rector-Brooks, Maksym Korablyov, Emmanuel Bengio, Moksh Jain, Andrei Cristian Nica, Tom Bosc, Yoshua Bengio, and Nikolay Malkin. Learning gflownets from partial episodes for improved convergence and stability. In *International Conference on Machine Learning*, pages 23467–23483. PMLR, 2023.

[44] Nikolay Malkin, Moksh Jain, Emmanuel Bengio, Chen Sun, and Yoshua Bengio. Trajectory balance: Improved credit assignment in gflownets. *Advances in Neural Information Processing Systems*, 35:5955–5967, 2022.

[45] Nikolay Malkin, Salem Lahlou, Tristan Deleu, Xu Ji, Edward J Hu, Katie E Everett, Dinghuai Zhang, and Yoshua Bengio. GFlownets and variational inference. In *The Eleventh International Conference on Learning Representations*, 2023.

[46] Michael Matthews, Michael Beukman, Benjamin Ellis, Mikayel Samvelyan, Matthew Jackson, Samuel Coward, and Jakob Foerster. Craftax: A lightning-fast benchmark for open-ended reinforcement learning. In *International Conference on Machine Learning (ICML)*, 2024.

[47] Mistal, Alex Hernández-García, Alexandra Volokhova, Alexandre AGM Duval, Yoshua Bengio, Divya Sharma, Pierre Luc Carrier, Michał Koziarski, and Victor Schmidt. Crystal-GFN: sampling materials with desirable properties and constraints. In *AI for Accelerated Materials Design - NeurIPS 2023 Workshop*, 2023.

[48] Sobhan Mohammadpour, Emmanuel Bengio, Emma Frejinger, and Pierre-Luc Bacon. Maximum entropy gflownets with soft q-learning. In *International Conference on Artificial Intelligence and Statistics*, pages 2593–2601. PMLR, 2024.

[49] Nikita Morozov, Ian Maksimov, Daniil Tiapkin, and Sergey Samsonov. Revisiting non-acyclic GFlowNets in discrete environments. In Aarti Singh, Maryam Fazel, Daniel Hsu, Simon Lacoste-Julien, Felix Berkenkamp, Tegan Maharaj, Kiri Wagstaff, and Jerry Zhu, editors, *Proceedings of the 42nd International Conference on Machine Learning*, volume 267 of *Proceedings of Machine Learning Research*, pages 44887–44910. PMLR, 13–19 Jul 2025.

[50] Nikita Morozov, Daniil Tiapkin, Sergey Samsonov, Alexey Naumov, and Dmitry Vetrov. Improving gflownets with monte carlo tree search. *arXiv preprint arXiv:2406.13655*, 2024.

[51] Radford M Neal et al. MCMC using Hamiltonian dynamics. *Handbook of Markov Chain Monte Carlo*, 2(11):2, 2011.

[52] Tri Minh Nguyen, Sherif Abdulkader Tawfik, Truyen Tran, Sunil Gupta, Santu Rana, and Svetha Venkatesh. Hierarchical GFlownet for crystal structure generation. In *AI for Accelerated Materials Design - NeurIPS 2023 Workshop*, 2023.

[53] Alexander Nikulin, Vladislav Kurenkov, Ilya Zisman, Viacheslav Sinii, Artem Agarkov, and Sergey Kolesnikov. XLand-minigrid: Scalable meta-reinforcement learning environments in JAX. In *Intrinsically-Motivated and Open-Ended Learning Workshop, NeurIPS2023*, 2023.

[54] Mizu Nishikawa-Toomey, Tristan Deleu, Jithendaraa Subramanian, Yoshua Bengio, and Laurent Charlin. Bayesian learning of causal structure and mechanisms with gflownets and variational bayes. *arXiv preprint arXiv:2211.02763*, 2022.

[55] Soichiro Nishimori. Jax-corl: Clean single-file implementations of offline rl algorithms in jax, 2024.

[56] Ling Pan, Nikolay Malkin, Dinghuai Zhang, and Yoshua Bengio. Better training of gflownets with local credit and incomplete trajectories. In *International Conference on Machine Learning*, pages 26878–26890. PMLR, 2023.

[57] Malak Pirtskhalava, Anthony A Amstrong, Maia Grigolava, Mindia Chubinidze, Evgenia Alimbarashvili, Boris Vishnepolsky, Andrei Gabrielian, Alex Rosenthal, Darrell E Hurt, and Michael Tartakovsky. Dbaasp v3: database of antimicrobial/cytotoxic activity and structure of peptides as a resource for development of new therapeutics. *Nucleic acids research*, 49(D1):D288–D297, 2021.

[58] Raghunathan Ramakrishnan, Pavlo O. Dral, Matthias Rupp, and O. Anatole von Lilienfeld. Quantum chemistry structures and properties of 134 kilo molecules. *Scientific Data*, 1(1):140022, 2014.

[59] Recursion. gflownet: Gflownet library specialized for graph and molecular data. <https://github.com/recursionpharma/gflownet>, 2025. GitHub repository.

[60] Christian P Robert, George Casella, and George Casella. *Monte Carlo statistical methods*, volume 2. Springer, 1999.

[61] Alexander Rutherford, Benjamin Ellis, Matteo Gallici, Jonathan Cook, Andrei Lupu, Garðar Ingvarsson, Timon Willi, Ravi Hammond, Akbir Khan, Christian Schroeder de Witt, Alexandra Souly, Saptarashmi Bandyopadhyay, Mikayel Samvelyan, Minqi Jiang, Robert Tjarko Lange, Shimon Whiteson, Bruno Lacerda, Nick Hawes, Tim Rocktäschel, Chris Lu, and Jakob Nicolaus Foerster. Jaxmarl: Multi-agent rl environments and algorithms in jax. In *The Thirty-eight Conference on Neural Information Processing Systems Datasets and Benchmarks Track*, 2024.

[62] Max W. Shen, Emmanuel Bengio, Ehsan Hajiramezanali, Andreas Loukas, Kyunghyun Cho, and Tommaso Biancalani. Towards understanding and improving gflownet training. In *Proceedings of the 40th International Conference on Machine Learning*, ICML’23. JMLR.org, 2023.

[63] Tony Shen, Seonghwan Seo, Grayson Lee, Mohit Pandey, Jason R Smith, Artem Cherkasov, Woo Youn Kim, and Martin Ester. TacoGFN: Target-conditioned GFlownet for structure-based drug design. *Transactions on Machine Learning Research*, 2024.

[64] Yujin Tang, Yingtao Tian, and David Ha. Evojax: Hardware-accelerated neuroevolution. *arXiv preprint arXiv:2202.05008*, 2022.

[65] Daniil Tiapkin, Nikita Morozov, Alexey Naumov, and Dmitry P Vetrov. Generative flow networks as entropy-regularized rl. In *International Conference on Artificial Intelligence and Statistics*, pages 4213–4221. PMLR, 2024.

[66] Edan Toledo, Laurence Midgley, Donal Byrne, Callum Rhys Tilbury, Matthew Macfarlane, Cyprien Courtot, and Alexandre Laterre. Flashbax: Streamlining experience replay buffers for reinforcement learning with jax, 2023.

[67] Ashish Vaswani, Noam Shazeer, Niki Parmar, Jakob Uszkoreit, Llion Jones, Aidan N Gomez, Łukasz Kaiser, and Illia Polosukhin. Attention is all you need. *Advances in neural information processing systems*, 30, 2017.

[68] Jian-Sheng Wang and Robert H Swendsen. Cluster monte carlo algorithms. *Physica A: Statistical Mechanics and its Applications*, 167(3):565–579, 1990.

[69] Mingze Yin, Hanjing Zhou, Yiheng Zhu, Jialu Wu, Wei Wu, Mingyang Li, Kun Fu, Zheng Wang, Chang-Yu Hsieh, Tingjun Hou, and Jian Wu. Synergy of gflownet and protein language model makes a diverse antibody designer. *Proceedings of the AAAI Conference on Artificial Intelligence*, 39(21):22164–22172, Apr. 2025.

[70] Dinghuai Zhang, Nikolay Malkin, Zhen Liu, Alexandra Volokhova, Aaron Courville, and Yoshua Bengio. Generative flow networks for discrete probabilistic modeling. In *International Conference on Machine Learning*, pages 26412–26428. PMLR, 2022.

- [71] Shuo Zhang, Yang Liu, and Lei Xie. Molecular mechanics-driven graph neural network with multiplex graph for molecular structures. *arXiv preprint arXiv:2011.07457*, 2020.
- [72] Ming Yang Zhou, Zichao Yan, Elliot Layne, Nikolay Malkin, Dinghuai Zhang, Moksh Jain, Mathieu Blanchette, and Yoshua Bengio. PhyloGFN: Phylogenetic inference with generative flow networks. In *The Twelfth International Conference on Learning Representations*, 2024.

Appendix

A Background

Generative Flow Networks. GFlowNets aim at sampling from a probability distribution over a finite discrete space \mathcal{X} given by $\pi(x) = \mathcal{R}(x)/Z$, where $\mathcal{R}: \mathcal{X} \rightarrow \mathbb{R}_{\geq 0}$ is the *GFlowNet reward*, and Z is the (typically unknown) normalizing constant.

To formally define a generation process in GFlowNets, we introduce a directed acyclic graph (DAG) $\mathcal{G} = (\mathcal{S}, \mathcal{E})$, where \mathcal{S} is a state space and $\mathcal{E} \subseteq \mathcal{S} \times \mathcal{S}$ is a set of edges (or transitions). There is exactly one state, s_0 , with no incoming edges, which we refer to as the *initial state*. All other states can be reached from s_0 , and the set of *terminal states* with no outgoing edges coincides with the space of interest \mathcal{X} . Non-terminal states $s \notin \mathcal{X}$ correspond to "incomplete" objects and edges $s \rightarrow s'$ represent adding "new components" to such objects, transforming s into s' . Let \mathcal{T} denote the set of all complete trajectories $\tau = (s_0, s_1, \dots, s_{n_\tau})$ in the graph, where τ is a sequence of states such that $(s_i \rightarrow s_{i+1}) \in \mathcal{E}$ and that starts at s_0 and finishes at some terminal state $s_{n_\tau} \in \mathcal{X}$. As a result, any complete trajectory can be viewed as a sequence of actions that constructs the object corresponding to s_{n_τ} starting from the "empty object" s_0 .

We say that a state s' is a child of a state s if there is an edge $(s \rightarrow s') \in \mathcal{E}$. In this case, we also say that s is a parent of s' . Next, for any state s , we introduce the *forward policy*, denoted by $\mathcal{P}_F(s'|s)$ for $(s \rightarrow s') \in \mathcal{E}$, as an arbitrary probability distribution over the set of children of the state s . In a similar fashion, we define the *backward policy* as an arbitrary probability distribution over the parents of a state s and denote it as $\mathcal{P}_B(s'|s)$, where $(s' \rightarrow s) \in \mathcal{E}$.

Given these two definitions, the main goal of GFlowNet training is a search for a pair of policies such that the induced distributions over complete trajectories in the forward and backward directions coincide:

$$\prod_{t=1}^{n_\tau} \mathcal{P}_F(s_t | s_{t-1}) = \frac{\mathcal{R}(s_{n_\tau})}{Z} \prod_{t=1}^{n_\tau} \mathcal{P}_B(s_{t-1} | s_t), \quad \forall \tau \in \mathcal{T}. \quad (1)$$

The relation (1) is known as the *trajectory balance constraint* [44]. We refer to the left and right-hand sides of (1) as to the forward and backward trajectory distributions and denote them as

$$\mathcal{P}_{\mathcal{T}}^{\mathcal{P}_F}(\tau) := \prod_{i=1}^{n_\tau} \mathcal{P}_F(s_i | s_{i-1}), \quad \mathcal{P}_{\mathcal{T}}^{\mathcal{P}_B}(\tau) := \frac{\mathcal{R}(s_{n_\tau})}{Z} \cdot \prod_{i=1}^{n_\tau} \mathcal{P}_B(s_{i-1} | s_i), \quad (2)$$

where $\tau = (s_0, s_1, \dots, s_{n_\tau}) \in \mathcal{T}$. If the condition (1) is satisfied for all complete trajectories, sampling a trajectory in the forward direction using \mathcal{P}_F will result in a terminal state being sampled with probability $\mathcal{R}(x)/Z$. We will call such \mathcal{P}_F a *proper* GFlowNet forward policy.

In practice, we train a model (usually a neural network) that parameterizes the forward policy (and possibly other auxiliary functions) to minimize an objective function that enforces the constraint (1) or its equivalent. The main existing objectives are *Detailed Balance* (DB, 3), *Trajectory*

Balance (TB, 44) and *Subtrajectory Balance* (SubTB, 43). The DB objective is defined as

$$\mathcal{L}_{\text{DB}}(\theta; s, s') = \left(\log \frac{F_\theta(s) \mathcal{P}_F(s'|s, \theta)}{F_\theta(s') \mathcal{P}_B(s|s', \theta)} \right)^2, \quad (3)$$

where $F_\theta(s)$ is a neural network that approximates the *flow* function of the state s , see [3, 43] for more details on the flow-based formalization of the GFlowNet problem. Using condition (1), the DB objective can be generalized to entire trajectory, yielding the TB objective:

$$\mathcal{L}_{\text{TB}}(\theta; \tau) = \left(\log \frac{Z_\theta \prod_{t=1}^{n_\tau} \mathcal{P}_F(s_t|s_{t-1}, \theta)}{\mathcal{R}(s_{n_\tau}) \prod_{t=1}^{n_\tau} \mathcal{P}_B(s_{t-1}|s_t, \theta)} \right)^2, \quad (4)$$

where Z_θ is a global constant estimating the normalizing constant Z . Finally, the SubTB objective is defined as

$$\mathcal{L}_{\text{SubTB}}(\theta; \tau) = \sum_{0 \leq j < k \leq n_\tau} w_{jk} \left(\log \frac{F_\theta(s_j) \prod_{t=j+1}^k \mathcal{P}_F(s_t|s_{t-1}, \theta)}{F_\theta(s_k) \prod_{t=j+1}^k \mathcal{P}_B(s_{t-1}|s_t, \theta)} \right)^2, \quad (5)$$

here $F_\theta(s)$ is substituted with $\mathcal{R}(s)$ for terminal states s , and w_{jk} is usually taken to be λ^{k-j} and then normalized to sum to 1. TB and DB objectives can be viewed as special cases of (5), which are obtained by only taking the term corresponding to the full trajectory or to individual transitions, respectively.

Some environments, such as phylogenetic tree generation, use the FLDB (Forward-Looking Detailed Balance) objective due to [56]. This loss applies for environments with rewards $\mathcal{R}(x) = \exp(-E(x))$ with $E(x)$ is the *energy function*, and the energy function is well defined for all states s , with the condition $E(s_0) = 0$. We then introduce the forward-looking flow function $\tilde{F}_\theta(s)$, defined for a state s via the flow function F :

$$\tilde{F}_\theta(s) := \exp(E(s)) F_\theta(s). \quad (6)$$

Using this function, we can rewrite the detailed balance constraint and obtain the forward-looking detailed balance (FLDB) constraint (see [56, Eq. 10],). Based on this constraint, we obtain the FLDB objective using the same techniques as in DB:

$$\mathcal{L}_{\text{FLDB}}(\theta; s, s') = \left(\log \frac{\tilde{F}_\theta(s) \mathcal{P}_F(s'|s, \theta)}{\tilde{F}_\theta(s') \mathcal{P}_B(s|s', \theta)} + E(s') - E(s) \right)^2. \quad (7)$$

All objectives allow either training the model in an on-policy regime using the trajectories sampled from \mathcal{P}_F or in an off-policy mode using the replay buffer or some exploration techniques. In addition, it is possible to either optimize \mathcal{P}_B along with \mathcal{P}_F or to use a fixed \mathcal{P}_B , e.g., the uniform distribution over parents of each state. One can show that given any fixed \mathcal{P}_B , there exists a unique \mathcal{P}_F that satisfies (1); see, e.g., [44].

We further write $P_\theta(x)$ for a marginal distribution over the terminal set, induced by the GFlowNet with the forward policy $\mathcal{P}_F(s'|s, \theta)$. We write $\hat{P}_\theta(x)$ for an estimate of $P_\theta(x)$, obtained with different environment-specific methods, detailed in further sections.

B Experiments

In this section, we provide comparisons between `gfnx` and previous implementations of GFlowNets on various environments. We use either `torchgfn` or author implementations of the benchmarks discussed below. Reported metrics are averaged across runs on at least 3 random seeds.

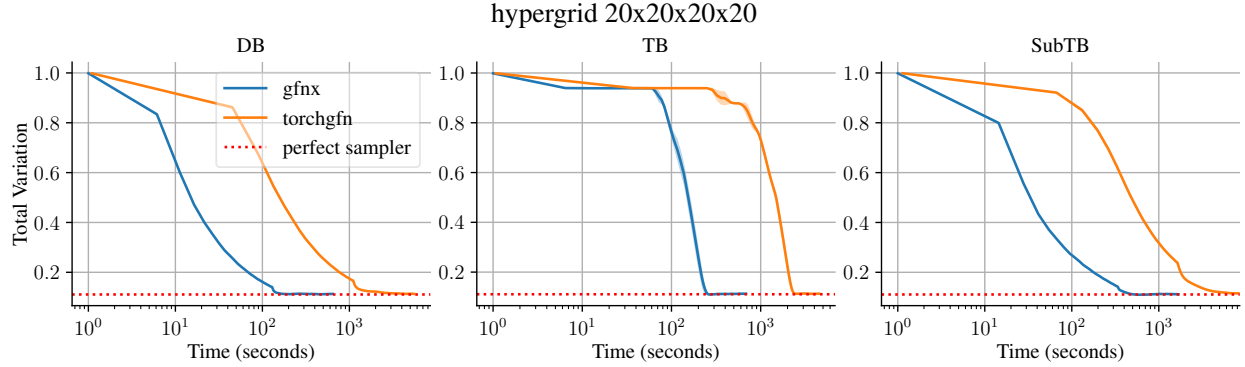


Figure 2: Total variation between true reward and empirical sample distributions versus total training time (in seconds). The same number of training iterations was used for different implementations. We use torch implementation from [39]. These experiments were performed on CPU.

B.1 Hypergrid

We implement a synthetic hypergrid environment introduced by [2]. It is a d -dimensional hypercube with a side length H . The state space consists of d -dimensional vectors $(s_1, \dots, s_d)^\top \in \{0, \dots, H-1\}^d$, with the initial state being $(0, \dots, 0)^\top$. For each state (s_1, \dots, s_{d-1}) , there are at most $d+1$ actions. The first action always corresponds to an exit action that transfers the state to its terminal copy, while the remaining d actions each increment one coordinate by 1 without leaving the grid. The number of terminal states is $|\mathcal{X}| = H^d$. There are 2^d regions with high rewards near the corners of the grid, while states outside have much lower rewards. The reward at a terminal state s with coordinates (s^1, \dots, s^D) is defined as

$$\mathcal{R}(s) = R_0 + R_1 \times \prod_{i=1}^D \mathbb{I}\left[0.25 < \left|\frac{s^i}{H-1} - 0.5\right| \right] + R_2 \times \prod_{i=1}^D \mathbb{I}\left[0.3 < \left|\frac{s^i}{H-1} - 0.5\right| < 0.4\right]. \quad (8)$$

For our experiments we use standard reward parameters ($R_0 = 10^{-3}$, $R_1 = 0.5$, $R_2 = 2.0$), taken from [2].

This environment is sufficiently small to benchmark algorithms on a CPU and to compute the target distribution in closed form, allowing us to directly examine the convergence of empirical distribution $P_\theta(x)$ to $\mathcal{R}(x)/Z$. Moreover, this gives us access to a perfect sampler that samples from the ground truth distribution of the reward function.

We conduct experiments on a 4-dimensional hypergrid with a side length of 20. As an evaluation metric, we use total variation distance of the true reward distribution and the empirical distribution of the last $2 \cdot 10^5$ terminal states sampled during training. Since we compute the metric using the empirical distribution of the sampler over a finite number of samples, this introduces a bias, so even a perfect sampler does not have a zero total variation metric. Therefore, we provide the metric of a perfect sampler for this environment. We compare our implementation against the `torchgfn` library [39] using the DB, TB and SubTB objectives.

Figure 2 presents the results. For all objectives, both implementations converge and yield the same total variation metric, while `gfnx` runs faster. Table 1 reports the exact performance of the libraries and shows that the `gfnx` implementation is at least about five times faster than `torchgfn` for this environment on CPU. We also provide additional experiments on 2-dimensional hypergrid 20×20 and 8-dimensional hypergrid with side length 10 in Table 2.

Objective	<code>torchgfn</code>	<code>gfnx</code>
DB	321.8 ± 2.5 it/s	3235.0 ± 86.7 it/s
TB	359.8 ± 13.1 it/s	1853.3 ± 14.9 it/s
SubTB	222.1 ± 1.4 it/s	2258.0 ± 53.6 it/s

(a) 2-dimensional hypergrid with a side length of 20.

Objective	<code>torchgfn</code>	<code>gfnx</code>
DB	209.6 ± 1.8 it/s	1453.6 ± 2.9 it/s
TB	225.3 ± 3.7 it/s	1443.8 ± 4.0 it/s
SubTB	143.6 ± 0.7 it/s	598.1 ± 3.4 it/s

(b) 8-dimensional hypergrid with a side length of 10.

Table 2: Iterations per second comparison between `torchgfn` [39] and `gfnx` libraries on small and large Hypergrid environments. Higher values indicate better performance. These experiments were performed on CPU.

Table 3: Hyperparameter choices for hypergrid experiments.

Hyperparameter	Value
Training trajectories	10^6
Learning rate	10^{-3}
Z learning rate for TB	10^{-1}
Adam optimizer $\beta, \varepsilon, \lambda$	$(0.9, 0.999), 10^{-8}, 0$
Number of hidden layers	2
Hidden embedding size	256
SubTB λ	0.9

All models are parameterized using an MLP with 2 hidden layers and 256 hidden units. We use the Adam optimizer with a learning rate of 10^{-3} and a batch size of 16 trajectories. For `SubTB`, we set $\lambda = 0.9$, following [43].

Hypergrid experiments were performed on an Intel Core i7-10700F CPU with 32 GB of RAM. Table 3 summarizes the chosen hyperparameters. To implement the first-in first-out buffer to store the transitions in order to evaluate an empirical distribution over terminals, we used `flashbox` library [66].

B.2 Sequential environments

We implement a number of sequential environments for the task of generating strings with a finite vocabulary and either fixed or variable length. Conceptually, there are several ways to model sequence generation:

- **Autoregressive generation (fixed length).** In this setting, sequence is generated step by step from left to right until a fixed length n is reached. Each step involves selecting the next symbol from a vocabulary of size m . The resulting state space thus consists of all partial sequences of length up to n , and the action space comprises m possible symbol choices at each step.
- **Autoregressive generation (variable length).** In this setting, sequences are generated autoregressively but can terminate before reaching the maximum length n . To enable variable-length outputs, we introduce a special *stop* action. The state space includes all strings of length up to n , while the action space contains the m symbols plus the stop action. \mathcal{P}_B then, remains degenerate, as per the nature of autoregressive MDP.

- **Prepend/append generation.** In this setting, a sequence of maximum length n is generated by adding symbols either to the beginning or to the end of the current string. At each step, one of m symbols is chosen from the vocabulary, along with a binary choice specifying whether to *prepend* or *append*. Thus, the action space consists of $2m$ possible actions, and the state space includes all sequences of length up to n .
- **Non-autoregressive generation.** In this setting, we generate fixed-length sequences (of length n) by selecting both a position and a symbol at each step. Initial state s_0 corresponds to the sequence of empty tokens \emptyset . The available actions correspond to choosing a position with an empty token and replacing it with a token from the given vocabulary. The action space can therefore be represented as all possible pairs (i, a) , where $i \in \{1, \dots, n\}$ denotes the position and $a \in \{1, \dots, m\}$ the symbol to insert.

Below we present a number of popular sequential GFlowNet environments

Bit sequences. The bit sequences environment [44] aims to generate binary strings of fixed length $n \in \mathbb{N}$. The action space and the vocabulary size depends on the hyperparameter k , which is responsible for a trade-off between the trajectory length and the action space size. Formally, we choose $k|n$, splitting the bit sequence into n/k blocks, each containing k bits. We implement the non-autoregressive version of the environment presented in [65], where at each step one chooses a position with an empty token and replaces it with a k -bit word. The reward function is defined as:

$$\mathcal{R}(x) = \exp \left\{ -\beta \min_{x' \in M} \frac{d(x, x')}{n} \right\},$$

where $d(x, x')$ is the Hamming distance between the strings x, x' , M is the reference set (mode set), and β is the reward exponent. We fix M in advance, and the learner has access only to the reward function, not to the set M itself. We generate the set M according to the procedure described in [44]. Namely, we choose the same size $|M| = 60$. We set

$$H = \{00000000', 11111111', 11110000', 00001111', 00111100'\}.$$

Each sequence in M is generated by randomly selecting $n/8$ elements from H with replacement and then concatenating them. The test set for evaluating reward correlations is generated by taking a mode and flipping i random bits in it, where this is repeated for every mode and for each $0 \leq i < n$.

We follow the evaluation setup of [65]. We measure Pearson correlation on the test set between $\mathcal{R}(x)$ and $\hat{P}_\theta(x)$, where the latter is a Monte Carlo estimate of the probability to sample x from the trained GFlowNet proposed in [70, 65]. Namely, we notice that

$$P_\theta(x) = \mathbb{E}_{\mathcal{P}_B(\tau|x)} \left[\frac{\mathcal{P}_F(\tau | \theta)}{\mathcal{P}_B(\tau | x)} \right],$$

and estimate $P_\theta(x)$ with its Monte-Carlo estimate $\hat{P}_\theta(x)$ based on $N = 10$ samples:

$$\hat{P}_\theta(x) = \frac{1}{N} \sum_{i=1}^N \frac{\mathcal{P}_F(\tau^i | \theta)}{\mathcal{P}_B(\tau^i | x)}, \quad \tau^i \sim \mathcal{P}_B(\tau | x).$$

Notice that any valid \mathcal{P}_B can be used here, but for each model, we take the \mathcal{P}_B that was fixed/trained alongside the corresponding \mathcal{P}_F since such a choice will lead to a lower estimate variance.

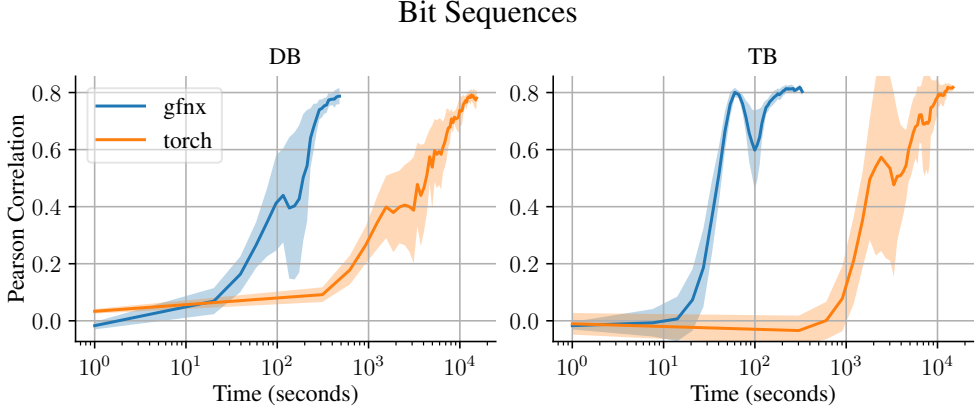


Figure 3: Comparison of `gfnx` and `torch` implementation [65] on the bit sequence generation task ($n = 120, k = 8$). Comparison of the performance in terms of the Pearson correlation coefficient between the terminating state log-probability and the log-reward on 7200 randomly sampled bit sequences (higher better). Curves were smoothed using a moving average for visual clarity. Experiments were performed on GPU using TB and DB objectives.

Table 4: Hyperparameter choices for Bit Sequences, TFBind8, and QM9 experiments.

Hyperparameter	Bit Sequences	TFBind8 and QM9
Training iterations	5×10^4	10^6
Learning rate	10^{-3}	5×10^{-4}
Z learning rate for TB		0.05
Adam optimizer $\beta, \varepsilon, \lambda$	$(0.9, 0.999), 10^{-8}, 10^{-5}$	$(0.9, 0.999), 10^{-8}, 0$
ε -uniform exploration	10^{-3}	1.0 linearly annealed to 0.0
Reward exponent	3	10
Batch size		16
Number of MLP layers	–	2
Number of transformer layers	3	–
Hidden embedding size	64	256
Dropout	0	–

We compare our implementation against PyTorch implementation from [65] using DB and TB objectives. Figure 3 presents the results. For bit sequences environment, `gfnx` implementation runs faster with the same metric values. Table 1 reports the exact performance of the implementations and shows that the `gfnx` implementation is at least 30 times faster than `torch` on GPU.

All models are parameterized as transformers [67] with 3 hidden layers, 8 attention heads, and a hidden dimension of 64. Each model is trained for 50,000 iterations and a batch size of 16 with AdamW optimizer with learning rate from 10^{-3} .

To closely follow the setting of previous works [44, 43, 65], we use ε -uniform exploration with $\varepsilon = 10^{-3}$. Each bit sequence experiment was performed on a single NVIDIA V100 GPU. Table 4 summarizes the chosen hyperparameters.

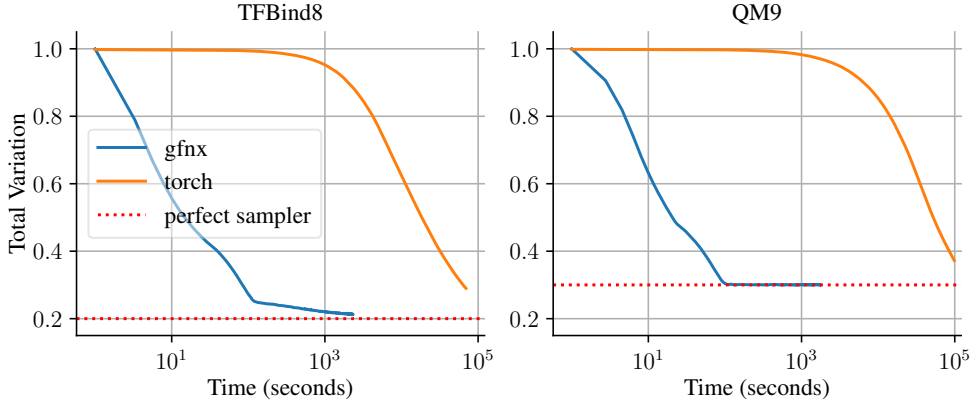


Figure 4: Total variation between true reward and empirical sample distributions versus total training time (in seconds) on TFBind8 and QM9 environments. We use torch implementation from [62]. Experiments were performed on CPU using the TB objective.

B.2.1 TFBind8 and QM9

TFBind8 environment evaluates DNA sequence design, where the goal is to generate length 8 sequences of nucleotides. The reward is wet-lab measured DNA binding activity to a human transcription factor, SIX6 [1]. Formally, this is an autoregressive sequence generation environment of fixed length 8 with a vocabulary of size 4 (corresponding to nucleotides A, C, G, and T).

QM9 is a small molecule generation environment. We use the prepend/append sequence formulation of this environment from [62]. This is a small version of the environment that uses 11 building blocks with 2 stems, and generates 5 blocks per molecule. Rewards are predictions of a proxy model trained on the QM9 dataset [58] to predict HOMO-LUMO gap [71]. It is worth mentioning that there exists a more complex atom-by-atom setup for this environment from [48], while we implement a sequential formulation from [62].

We compare our implementation against PyTorch implementation from [62] using TB objective. As an evaluation metric, we use total variation distance of the true reward distribution and the empirical distribution of the last $2 \cdot 10^5$ terminal states sampled during training. For both environments, we use pre-trained weights for the proxy model from [62].

These environments are sufficiently small to allow benchmarking algorithms on a CPU and enable computation of the target distribution in closed form. Moreover, this gives us access to a perfect sampler that samples from the ground truth distribution of the reward proxy model. Since we compute the metric using the empirical distribution of the sampler, this introduces high variance, so even a perfect sampler does not have a zero total variation metric. Therefore, we provide the metric of a perfect sampler for these environments.

Figure 4 presents the results. For both TFBind8 and QM9 environments, **gfnx** implementation runs faster and more over get the better total variation metric with the same number of sampling trajectories. Table 1 reports the performance of implementations and shows that the **gfnx** implementation is at least 30 times faster than **torch** for this environments on CPU.

All models are parameterized using an MLP with 2 hidden layers and 256 hidden units. We use the Adam optimizer with a learning rate of $5 \cdot 10^{-4}$ and a batch size of 16 trajectories. The learning rate for Z is fixed at 0.05 for all experiments. We use ε -uniform exploration with $\varepsilon = 1.0$ that linearly anneal to zero over the $5 \cdot 10^4$ steps. TFBind8 and QM9 experiments were performed on an Intel Core i7-10700F CPU with 32 GB of RAM. Table 4 summarizes the chosen hyperparameters.

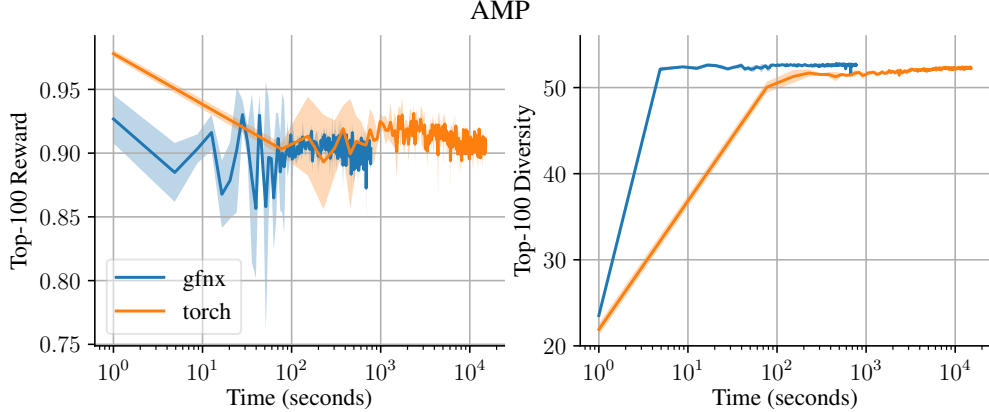


Figure 5: Top-100 reward and diversity versus total training time (in seconds) on AMP environment. We use torch implementation from [29]. The experiment was performed on GPU using the TB objective.

B.2.2 AMP

In the AMP task [57], the goal is to generate peptides with antimicrobial properties. In our setup, we use an autoregressive environment with variable sequence lengths (up to a maximum of 60) and a vocabulary consisting of 20 amino acids.

Table 5: Hyperparameter choices for AMP experiment.

Hyperparameter	Value
Training iterations	2×10^4
Learning rate	10^{-3}
Z learning rate for TB	0.64
Adam optimizer $\beta, \varepsilon, \lambda$	$(0.9, 0.999), 10^{-8}, 10^{-5}$
ε -uniform exploration	10^{-3}
Number of transformer layers	3
Hidden embedding size	64
Dropout	0.0

We use a proxy reward model $\mathcal{R}_\varphi(x)$ based on a classifier trained on a dataset of 3219 AMP and 4611 non-AMP sequences from the DBAASP database [57]. Our experimental setting is identical to the one of [44]. The reward function is, therefore,

$$\mathcal{R}_\varphi(x) = \max(\sigma(f_\varphi(x)), r_{\min}),$$

where $r_{\min} > 0$ is the hyperparameter, $\sigma(\cdot)$ is a sigmoid function, and $f_\varphi(x)$ is a classifier logit.

We also employ the evaluation setup used in ([44], [29], [43]). We compare our implementation against PyTorch implementation from [29] using TB objective. Figure 5 presents the results. For AMP environment, **gfnx** implementation runs faster with the approximately same metric values. Table 1 reports the exact performance of the implementations and shows that the **gfnx** implementation is at least 19 times faster than **torch** for this environment on GPU.

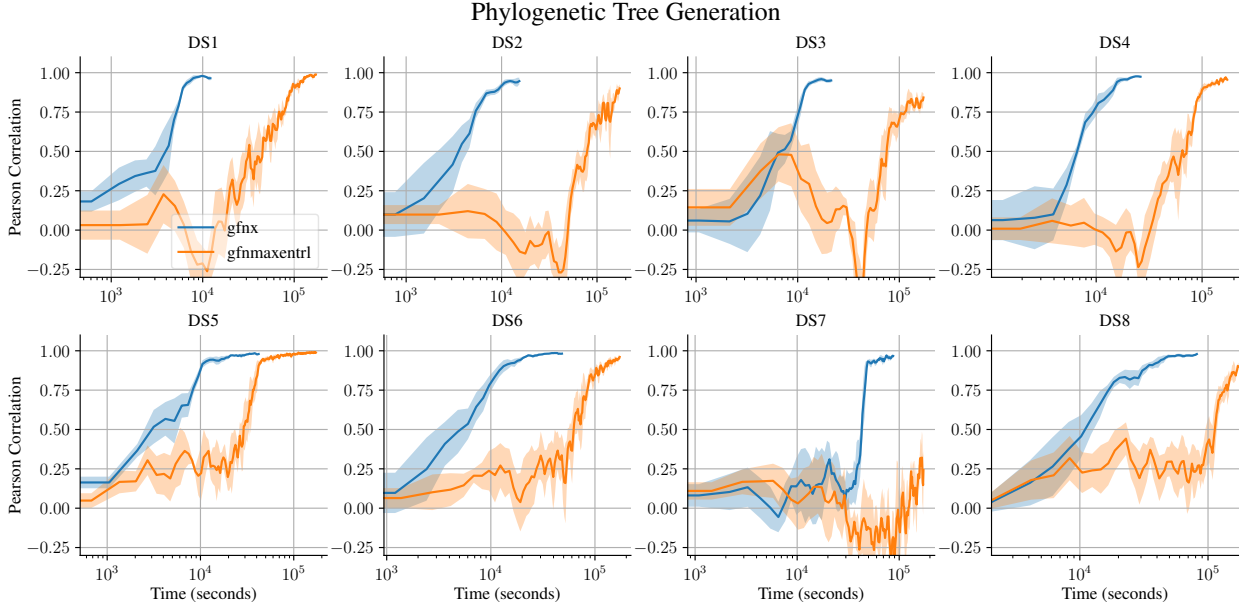


Figure 6: Comparison of gfnx and [15] paper implementation on the phylogenetic tree generation task. Comparison of the performance in terms of the Pearson correlation coefficient between the terminating state log-probability and the log-reward on 32 randomly sampled trees (higher better). Each run is limited to 48 hours. Curves were smoothed using a moving average for visual clarity. Experiments were performed on GPU using the FLDB objective.

All models are parameterized as Transformers [67] with 3 hidden layers, 8 attention heads, and a hidden dimension of 64. Each model is trained for 50,000 iterations and a batch size of 16 with AdamW optimizer with learning rate from 10^{-3} . We use ε -uniform exploration with $\varepsilon = 10^{-2}$ and initialize $\log Z = 150$ as in [29].

For transition-level losses (e.g., DB), we also treat terminal and nonterminal states differently. We penalize loss highly on terminal states. We use $\lambda = 25$ as the penalization factor for terminal states. Each AMP experiment was performed on a single NVIDIA V100 GPU. Table 5 summarizes the chosen hyperparameters.

B.3 Phylogenetic trees generation

A phylogenetic tree is a rooted binary tree whose leaves correspond to the observed species. We follow [72] and model the construction of such trees as a sequential decision process. The initial state s_0 is given by a forest of n singleton trees, each containing one species. At each step, the agent selects two trees from the forest and merges them under a new common ancestor, resulting in a new forest with one fewer tree. After $n - 1$ steps, this process yields a complete rooted binary tree over all n species. The state space therefore consists of all possible forests that can be obtained along the way, while actions correspond to pairwise merges. The reward of a terminating state x is defined as

$$\mathcal{R}(x) = \exp(-M(x)/\alpha),$$

where $\alpha > 0$ is a temperature parameter, and $M(x)$ is the parsimony score of the tree, i.e., the minimum number of mutations required to explain the observed species under x . This reward structure induces a Gibbs distribution over phylogenetic trees, strongly favoring trees with fewer

Table 6: Hyperparameter choices for phylogenetic trees generation experiments.

Hyperparameter	Value
Reward temperature α	4
Reward constant C	$\{5800, 8000, 8800, 3500, 2300, 2300, 12500, 2800\}$
Training trajectories	3.2×10^6
Learning rate	$3 \cdot 10^{-4}$ cosinely annealed to 10^{-5}
Warmup steps	5000
Adam optimizer $\beta, \varepsilon, \lambda$	$(0.9, 0.999), 10^{-8}, 0$
ε -uniform exploration	1.0 linearly annealed to 0.0 for half of training
Number of attention heads	8
Number of transformer layers	6
Hidden size	32
Dropout	0.01
Embedding size	128
Hidden embedding size	256
Number of MLP layers	3
MLP hidden size	256

evolutionary steps while still assigning non-zero probability to sub-optimal candidates. In this formulation, branch lengths are not modeled and we consider only the topology of the tree.

We conduct experiments on 8 datasets introduced in [72]. As an evaluation metric, we use the Pearson correlation coefficient between the terminating state log-probability and the log-reward of 32 randomly sampled trees. We compare our implementation against the JAX implementation of phylogenetic tree generation from the `gfnmaxentrl` paper [15] using the `FLDB` objective [56]. To compute correlation, we use the same Monte Carlo estimate as in the bit sequence task, we compute correlation on sampled trees from the current policy. The code in [15] does not provide computation of this metric, so we report self-implemented metrics.

Figure 6 presents the results. All implementations have a compute budget of 48 hours and were stopped after reaching it. The [15] implementation reached the time limit on all datasets, whereas `gfnx` works fast and finished in time. For most datasets both implementations converged to approximately the same metrics before being stopped. For the DS7 dataset, training proved particularly challenging and the `gfnmaxentrl` implementation did not converge in time. A more accurate comparison of performance is shown in Table 1. The `gfnx` implementation is mostly at least 10 times faster than `gfnmaxentrl`, due to the full training pipeline being written in JAX, whereas the `gfnmaxentrl` environment was written in NumPy and does not work on GPU.

For training stability we multiply the reward by a constant, depending on the dataset:

$$\mathcal{R}(T) = \exp\left(\frac{C - M(T)}{\alpha}\right).$$

We choose the hyperparameter C as in [15], for datasets DS1–DS8, we set it to 5800, 8000, 8800, 3500, 2300, 2300, 12500, and 2800, respectively. For all datasets, we use a constant reward temperature α set to 4.

All models are parameterized as Transformers [67] with 6 hidden layers, 8 attention heads, a hidden dimension of 32, and a feed-forward hidden dimension of 128. Each model is trained for $3.2 \cdot 10^6$ trajectories with the Adam optimizer. The batch size is set to 32 for the DS1–DS4 datasets,

to 16 for the DS5, DS6, and DS8 datasets, and to 8 for the DS7 dataset. Target models are updated using exponential moving averaging with $\tau = 0.005$.

To be more consistent with experiments for other environments, all experiments are conducted without a replay buffer, unlike the standard implementation in [15]. Each phylogenetic tree experiment was performed on a single NVIDIA V100 GPU. Table 6 summarizes the chosen hyperparameters.

B.4 Structure learning of Bayesian networks

We consider the task of Bayesian structure learning. A Bayesian network is a probabilistic graphical model over random variables $\{X_1, \dots, X_d\}$, where the joint distribution factorizes according to a DAG G as

$$P(X_1, \dots, X_d) = \prod_{k=1}^d P(X_k | \text{Pa}_G(X_k)), \quad (9)$$

with $\text{Pa}_G(X_k)$ the parent set of X_k in G . The goal of Bayesian structure learning is to approximate the posterior

$$P(G | \mathcal{D}) \propto P(\mathcal{D} | G)P(G), \quad (10)$$

where \mathcal{D} denotes the observed dataset. We assume that the samples in \mathcal{D} are i.i.d., fully-observed. We use the setting where \mathcal{D} is generated under Erdős–Rényi model. We also assume a uniform prior over structures and implement both the Bayesian metric for Gaussian networks having score equivalence (BGe) [19] and linear Gaussian [54] scores as marginal likelihoods $P(\mathcal{D} | G)$.

The environment is defined as a sequential process that constructs a DAG by adding edges one at a time, while enforcing acyclicity by maintaining an incrementally updated adjacency matrix and transitive closure similar to [14]. A special stop action yields a terminal state corresponding to a valid DAG with a reward term that is given by

$$\log \mathcal{R}(G) = \log P(\mathcal{D} | G) + \log P(G). \quad (11)$$

Since in the environment every state can be terminal, we can employ Modified Detailed Balance (MDB) [14] algorithm for learning the posterior distribution. We also take the advantage of the reward structure for an efficient computation of the delta score, required by the MDB loss.

Experiments are conducted on 20 random Erdős–Rényi ground-truth graphs with expected in-degree 1, where for each graph we generate 100 samples by ancestral sampling. This problem is typically studied with $d = 5$ nodes, although settings with $d = 20$ or more are also possible. This environment is benchmarked only on GPU, as our models include deep architectures such as transformers and graph neural networks. We evaluate methods using Jensen–Shannon divergence between the learned and exact distributions over sampled DAGs. Additionally we implement correlation scores over path, edge, and Markov blanket marginals.

Local Scores and Modularity. A fundamental property of Bayesian structure learning is the *modularity* of both the structure prior $P(G)$ and the parameter prior $P(\varphi | G)$ [22, 9]. Under this assumption, the score of a graph decomposes into independent contributions from each variable given its parent set. Specifically, for a Bayesian network with DAG G over d nodes, the log-reward admits the additive form

$$\log \mathcal{R}(G) = \sum_{j=1}^d \text{LocalScore}(X_j | \text{Pa}_G(X_j)), \quad (12)$$

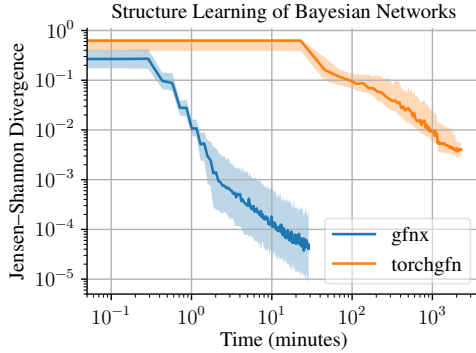


Figure 7: Jensen–Shannon divergence between true reward and empirical sample distributions versus total training time (in minutes). We use torch implementation from [39]. The experiment was performed on GPU using the MDB objective.

where each term $\text{LocalScore}(X_j \mid \text{Pa}_G(X_j))$ depends only on X_j and its parents. Standard Bayesian scores such as Linear Gaussian and BGe satisfy this decomposition.

Modularity implies that reward updates are computationally efficient. When an edge $X_i \rightarrow X_j$ is added to the graph, all local scores remain unchanged except for that of X_j . Consequently, the change in log-reward reduces to

$$\log \mathcal{R}(G') - \log \mathcal{R}(G) = \text{LocalScore}(X_j \mid \text{Pa}_G(X_j) \cup \{X_i\}) - \text{LocalScore}(X_j \mid \text{Pa}_G(X_j)), \quad (13)$$

a quantity referred to as the *delta score* or *incremental value* [18]. The delta score requires updating only a single local component, making it efficient to compute. This property is widely used in structure learning search algorithms [10, 36], and in our setting enables efficient computation of rewards within the GFlowNet training objective.

Dataset Generation Process. For our experiments, datasets are generated from randomly sampled ground-truth Bayesian networks. Each ground-truth DAG G^* is sampled from an Erdős–Rényi distribution with $d = 5$ nodes and an expected in-degree of 1. Conditional probability distributions are assumed to be linear-Gaussian: for each variable X_j , given its parents $\text{Pa}_{G^*}(X_j)$, we define

$$X_j \mid \text{Pa}_{G^*}(X_j) \sim \mathcal{N} \left(\sum_{i \in \text{Pa}_{G^*}(X_j)} w_{ij} X_i, \sigma_j^2 \right), \quad (14)$$

where the weights w_{ij} are drawn according to $w_{ij} \sim \mathcal{N}(0, 1)$ and the noise variances are fixed to $\sigma_j^2 = 0.1$. Data \mathcal{D} is then generated by ancestral sampling: nodes are ordered topologically according to G^* , and each variable is sampled conditionally on its parents. For each DAG, we generate 100 observations in this way.

This procedure is repeated for 20 different random seeds, producing a collection of datasets associated with 20 distinct Erdős–Rényi graphs. Each dataset therefore consists of 100 samples from a linear-Gaussian Bayesian network with known ground-truth structure, which enables exact posterior computation and comparison against learned distributions.

Online Mask Updates. To enforce acyclicity efficiently, we maintain two structures for each DAG G : the adjacency matrix of G , and the adjacency matrix of the transitive closure of G^\top (the

Table 7: Hyperparameter choices for structure learning of Bayesian networks experiments.

Hyperparameter	Value
Training steps	100000
Batch size	128
Learning rate	10^{-4}
ϵ -uniform exploration	1.0 linearly annealed to 0.1 for half of training
Target network update frequency	1000
Number of GNN layers	1
Number of MLP layers	2
Embedding size	128
Hidden size	128
Number of transformer heads	4

transpose graph obtained by reversing all edge directions). The mask of legal actions is derived from these components: it excludes (i) edges already present in G , and (ii) edges whose addition would create a cycle according to the transitive closure. When a new edge $(u \rightarrow v)$ is added, the update is performed online by (1) setting the corresponding entry in the adjacency matrix, and (2) updating the transitive closure of G^T via the outer product of the column of v and the row of u , applied as a binary OR to the existing closure. This update rule ensures correctness and requires only $O(d^2)$ time per edge addition, avoiding expensive cycle checks at every step.

Evaluation Metrics and Structural Features. We compare the learned distribution over DAGs with the exact posterior using the Jensen–Shannon divergence (JSD). We also provide an implementation of structural feature marginals correlations. Since the number of DAGs with $d = 5$ nodes is finite (29,281), all probabilities can be computed exactly by enumeration.

Figure 7 presents the results. All runs were given a 48-hour compute budget. The `torchgfn` baseline was trained with its replay-buffer implementation (the only stable variant), while `gfnx` was evaluated in a fully on-policy setting, which is substantially more computationally demanding. Despite this disadvantage, `gfnx` converges faster and reaches lower JSD, outperforming `torchgfn` by roughly a factor of $79\times$ in wall-clock efficiency under the BGe score. Both methods follow comparable learning trajectories, but `torchgfn` approaches the time limit well before matching the threshold score achieved by `gfnx`. Table 7 summarizes the chosen hyperparameters.

Jensen–Shannon divergence. For two distributions P and Q over the same support, the JSD is defined as

$$\text{JSD}(P \parallel Q) = \frac{1}{2} \text{KL}(P \parallel M) + \frac{1}{2} \text{KL}(Q \parallel M), \quad (15)$$

where $M = \frac{1}{2}(P + Q)$ and KL denotes the Kullback–Leibler divergence.

Edge features. For nodes X_i, X_j , the marginal probability of the edge feature $X_i \rightarrow X_j$ is

$$P(X_i \rightarrow X_j \mid \mathcal{D}) = \sum_G \mathbf{1}(X_i \rightarrow X_j \in G) P(G \mid \mathcal{D}). \quad (16)$$

Path features. For nodes X_i, X_j , the path feature $X_i \rightsquigarrow X_j$ indicates the existence of a directed path from X_i to X_j . Its marginal probability is

$$P(X_i \rightsquigarrow X_j \mid \mathcal{D}) = \sum_G \mathbf{1}(X_i \rightsquigarrow X_j \in G) P(G \mid \mathcal{D}). \quad (17)$$

Markov blanket features. For nodes X_i, X_j , the Markov blanket feature $X_i \sim_M X_j$ indicates that X_i belongs to the Markov blanket of X_j , i.e. X_i is either a parent, a child, or a co-parent of X_j . Its marginal probability is

$$P(X_i \sim_M X_j \mid \mathcal{D}) = \sum_G \mathbf{1}(X_i \sim_M X_j \in G) P(G \mid \mathcal{D}). \quad (18)$$

B.5 Ising model

We consider the problem of jointly learning an energy-based reward model (EBM) and a generative policy, given only samples stored in a dataset. An example of such a setting is learning the interaction matrix of an Ising model [27] together with a corresponding GFlowNet sampler, as explored in [70]. The proposed algorithm alternates updates between a Generative Flow Network and an energy model. A trajectory is generated either from the current forward policy, $\tau \sim P_F(\tau)$, with probability α (a hyperparameter of the procedure), or by first sampling a random data point \mathbf{x}_i from the dataset and then generating a full trajectory using the backward policy, $\tau \sim P_B(\tau \mid \mathbf{x}_i)$, with probability $1 - \alpha$. The GFlowNet is then updated according to Equation 4, using the current approximation of the energy-based reward model, $R(\mathbf{x}) = \exp(-\mathcal{E}(\mathbf{x}; \varphi))$.

The second step of the algorithm updates the parameters of the EBM. A common approach employs the contrastive divergence loss [24], which yields the following stochastic gradient:

$$\mathbb{E}_{\mathbf{x} \sim p_{\text{data}}(\mathbf{x})} [\nabla_{\varphi} \mathcal{E}_{\varphi}(\mathbf{x}) - \mathbb{E}_{\mathbf{x}' \sim q_K(\mathbf{x}' \mid \mathbf{x})} [\nabla_{\varphi} \mathcal{E}_{\varphi}(\mathbf{x}')]]. \quad (19)$$

In the context of Generative Flow Networks, the conditional distribution in the second term, $q_K(\mathbf{x}' \mid \mathbf{x})$, is obtained by performing K backward steps from the true sample \mathbf{x} using the backward policy $P_B(\cdot \mid \mathbf{x})$, followed by K forward steps using the forward policy P_F . The resulting sample \mathbf{x}' is then either accepted or rejected according to the acceptance probability:

$$A(\mathbf{x} \rightarrow \mathbf{x}') = \min \left[1, \frac{e^{-\mathcal{E}_{\varphi}(\mathbf{x}')}}{e^{-\mathcal{E}_{\varphi}(\mathbf{x})}} \frac{P_B(\tau \mid \mathbf{x}) P_F(\tau')}{P_B(\tau' \mid \mathbf{x}') P_F(\tau)} \right]. \quad (20)$$

Further details on the algorithm can be found in [70].

In our framework, we consider an Ising model defined on a given interaction graph with $D = N^2$ spins $\mathbf{x}^i \in \{-1, +1\}$ and energy function

$$\mathcal{E}_J(\mathbf{x}) = -\mathbf{x}^T J \mathbf{x}, \quad J \in \mathbb{R}^{D \times D}. \quad (21)$$

This defines a probability distribution over lattice configurations:

$$P(\mathbf{x}) \propto \exp(-\mathcal{E}_J(\mathbf{x})), \quad \mathbf{x} \in \{-1, +1\}^D. \quad (22)$$

Following [70], we model sampling from the corresponding Gibbs distribution as a GFlowNet environment over partial assignments. States are represented as ternary vectors $s \in \{-1, +1, \emptyset\}^D$, with the initial state $s_0 = (\emptyset, \dots, \emptyset)$. At each step, an action selects an unassigned site and sets

Method \ σ	$D = 10^2$					$D = 9^2$	
	0.1	0.2	0.3	0.4	0.5	-0.1	-0.2
EB-GFN (gfnx)	4.93 ± 0.25	4.48 ± 0.3	4.05 ± 0.03	3.26 ± 0.06	2.72 ± 0.04	3.79 ± 0.15	3.98 ± 0.01

Table 8: Mean negative log-RMSE (higher is better) between data-generating matrix J and learned matrix J_φ for different values of σ .

Table 9: Hyperparameter choices for Ising model experiments.

Hyperparameter	Value
Training steps	20000
Batch size	256
MLP hidden size	256
MLP depth	4
Number of true data samples	2000

its spin to -1 or $+1$; the backward policy, conversely, removes a previously assigned spin. After D steps, the process terminates at a full configuration $\mathbf{x} \in \{-1, +1\}^D$.

We define the true interaction matrix as $J = \sigma A_N$, where $\sigma \in \mathbb{R}$ and A_N is the adjacency matrix of a toroidal lattice with side length N . Experiments are conducted on lattices with side $N = 9$ and negative couplings $\sigma \in \{-0.1, -0.2\}$, and with $N = 10$ and positive couplings $\sigma \in \{0.1, 0.2, 0.3, 0.4, 0.5\}$. We also set $K = D$, so that $q_K(\mathbf{x}'|\mathbf{x}) = P_T(\mathbf{x}')$, where $P_T(\mathbf{x}')$ denotes the marginal probability of sampling \mathbf{x}' from the GFlowNet.

Table 8 reports the mean negative log-RMSE between the learned interaction matrix and the true lattice couplings for various values of σ . This is the only available open-source implementation of the EB-GFN setting from [70]. The scores align with the baselines reported in [70], though they differ from the exact numbers of their original implementation. Performance remains stable across lattice sizes and coupling strengths, with higher accuracy for weaker interactions.

To generate the dataset of true samples, we employ MCMC-based methods, including the Wolff algorithm [68] and Heat Bath Parallel Tempering [26]. Table 9 summarizes the chosen hyperparameters. We follow the same hyperparameter search procedure, introduced in [70]. Note that, according to their work, the training procedure stops when the error between the trained J_φ and the true J reaches its minimum.